Check for updates

Mixed-ligand-functionalized silicon–germanium alloy nanocrystals with improved carrier mobilities†

Linfeng Wei,[a] Haoyuan Zhang,[b] Lei Shi [iD] [b] and Zhenyu Yang [iD] *[a,c]

Silicon–germanium (SiGe) alloy nanocrystals (NCs) are promising for advanced optoelectronic applications due to their highly tunable composition and photophysical behaviors. The homogenous dispersion of Si and Ge atoms on the surfaces of SiGe NCs adds a degree of freedom for manipulating the surface chemistry of this type of alloy material. However, the difference in the reactivity between Si and Ge atoms brings additional difficulty in selecting appropriate surface ligands to passivate SiGe NCs. Here we report a mixed-ligand functionalization approach to passivate SiGe NCs effectively. Octadecene and oleylamine molecules serve as co-ligands to cap the surface Si and Ge atoms, respectively, yielding colloidally stable SiGe NCs with high solution dispersity and stable intrinsic near-infrared emission with a microsecond-scale lifetime decay. The resulting particles also show improved hole and electron mobilities of up to 1.1×10^{-6} cm^2 V^{-1} s^{-1} and 6.3×10^{-6} cm^2 V^{-1} s^{-1}, 2.2 and 1.2 times improvement over the particles only passivated by octadecene ligands.

[a]MOE Laboratory of Bioinorganic and Synthetic Chemistry, Lehn Institute of Functional Materials, School of Chemistry, IGCME, Sun Yat-sen University, Guangzhou 510275, China. E-mail: yangzhy63@mail.sysu.edu.cn
[b]State Key Laboratory of Optoelectronic Materials and Technologies, Nanotechnology Research Center, Guangdong Basic Research Center of Excellence for Functional Molecular Engineering, School of Materials Science and Engineering, Sun Yat-sen University, Guangzhou 510275, P. R. China
[c]Nanchang Research Institute, Sun Yat-sen University, Nanchang 330096, China
† Electronic supplementary information (ESI) available: The experimental details of the preparation of functionalized SiGe NCs and additional material characterization. See DOI: https://doi.org/10.1039/d3nr06008j

Zhenyu (Kevin) Yang obtained his B.Sc. in Chemistry from Nankai University in 2009 and completed his Ph.D. in Chemistry at the University of Alberta in 2014, under the supervision of Prof. Jonathan Veinot. Following this, from 2014 to 2018, he worked as a postdoctoral research fellow with Prof. Edward Sargent at the University of Toronto. In 2018, Kevin joined the School of Chemistry at Sun Yat-sen University as a Professor. His research is primarily focused on the synthesis and surface chemistry of quantum dots and the development of solution-processed optoelectronic devices, including light-emitting devices and photovoltaics.

Zhenyu Yang

Introduction

Among the emerging semiconducting nanomaterials, silicon nanocrystals (Si NCs) are of great interest due to their size- and surface-tunable photoluminescence, high biocompatibility, and high solution processability.[1–4] The incorporation of the isovalent element germanium in the silicon lattice adds another degree of freedom in the preparation of silicon–germanium (SiGe) alloy nanostructures with modified band structures and optoelectronic properties for potential applications in photodetectors,[5,6] field-effect transistors (FETs)[7] and photovoltaics.[8]

A variety of synthetic approaches have been developed for preparing SiGe NCs, including physical and chemical vapor deposition,[9] molecular beam epitaxy,[10,11] radio frequency co-sputtering,[12,13] nonthermal plasma pyrolysis,[14] and solid-state thermal disproportionation,[15,16] Most of these methods (and their subsequent processes) allow the formation of well-defined, homogeneous mixed SiGe alloy particles with highly reactive surface bonds (such as Si–H, Ge–H, Si–X, Ge–X, X = Cl, Br).[3,15,17] To avoid undesired oxidation and to enhance the compatibility with commonly used solvents, it is necessary to chemically modify these active surface bonds with organic ligands to form more robust alternative bonds.[16,18]

Driven by external sources such as heat, light, and radical initiators, surface modification approaches offer efficient passivation on Group 14 nanomaterials such as Si and Ge NCs.[2,19] Although the similarities between the Si and Ge surfaces are apparent, challenges still exist in functionalizing SiGe alloy NCs effectively. This may be due to the significant differences

in the bond dissociation energy and chemical reactivity when interacting with specific ligands between Si- and Ge-based surface bonds.[20] On the other hand, the competing reactions, such as the potential oxidation and spontaneous surface bond dissociation of the highly reactive linkages on Ge atoms, may occur and induce poorly functionalized SiGe surfaces. A general method to effectively functionalize Si and Ge atoms on SiGe NCs has yet to be demonstrated.

Here, we report a set of wet chemistry approaches to effectively passivate SiGe alloy NCs with hybrid ligands. Two types of reactions, radical-driven hydrosilylation/hydrogermanation and the interaction with organic amines, were applied together to substitute the original Si–H and Ge–H bonds on the SiGe NC surfaces with more robust chemical linkages such as Si–C, Si–N, and Ge–N bonds. The functionalized SiGe particles showed a uniform morphology with a significantly improved solution dispersity. The functionalized SiGe NCs showed lower surface oxidation and had intense photoluminescence in the near-infrared (NIR) region with a microsecond-scaled lifetime decay. In addition, the mixed-ligand (ML) functionalized particles show substantially improved hole and electron mobilities compared to the samples capped with conventional alkyl ligands, indicating the efficient surface passivation of SiGe NCs *via* the ML functionalization strategy.

Results and discussion

The synthetic method of SiGe NCs was inspired by a reported protocol about Ge NC preparation[21] and is described in the ESI† and Fig. 1a. Briefly, the co-hydrolysis of triethoxysilane (TriEOS) and tetraethoxygermane (TEOG) in a methanol/HNO₃

aqueous solution and the subsequent condensation processes yielded a homogenous cloudy suspension. After aging, a white gel-like product was isolated and dried to form an amorphous siloxane–germoxane copolymer $(HSiO_{1.5})_m(GeO_2)_n$. The subsequent thermal annealing of the copolymer under a slightly reducing atmosphere induced the disproportionation of Si^{3+} and the reduction of Ge^{4+}, yielding a homogenous dark-grey powdery composite containing crystalline germanium (c-Ge) and SiGe NCs embedded in an amorphous germanium silicon oxide (GSO) matrix (Fig. 1b and c).

X-ray diffraction (XRD) characterization was applied to confirm the crystallinity of the product. A set of diffraction signals at 28.1°, 46.7°, and 55.4° arise from a diamond-type crystal with the lattice constant intermediate to bulk silicon and germanium (Fig. 1c), indicating the formation of SiGe NCs. An empirically modified version of Vegard's law (Note S1 in the ESI†) was applied to calculate the alloy composition of $Si_{0.7}Ge_{0.3}$ obtained from the thermally annealed composite (Fig. S1 and Table S2†). Another set of diffraction signals at 27.2°, 45.3°, and 53.7° can be assigned to the (111), (220), and (311) facets of diamond structural germanium. The formation of the Ge crystal is not unexpected as Ge^{4+} is readily reduced to Ge^0 at high temperatures.[21,22]

We therefore developed a two-step etching process to obtain pure SiGe NCs from the annealed composite. Firstly, H_2O_2 solution was applied to completely oxidize and dissolve the crystalline germanium chunks, whereas the components embedded in the oxide matrix shall not be affected. After H_2O_2 etching, the color of the composite merely changed. In contrast, the Ge diffraction peaks disappeared from the XRD pattern, indicating the effective removal of c-Ge and the successful preservation of SiGe domains (Fig. 1c). In the second
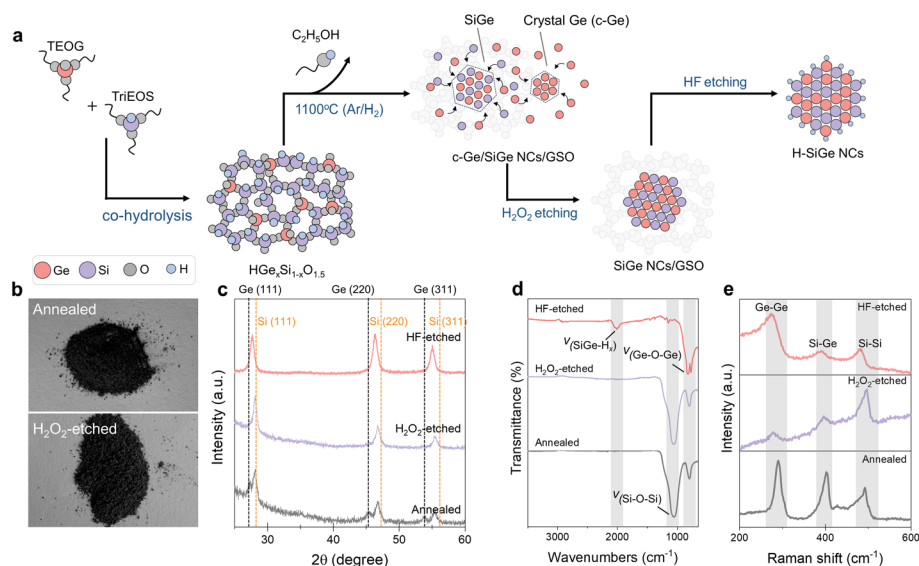

Fig. 1 Solid-state synthesis and materials characterizations of SiGe NCs. (a) Schematic illustration of the processes in the preparation of SiGe NCs. (b) Images of the c-Ge/SiGe NC/GSO composite before and after H_2O_2 etching. (c) XRD, (d) FT-IR, and (e) Raman results of the pristine c-Ge/SiGe NC/GSO sample and the samples after H_2O_2 etching and two-step etching (*i.e.*, H_2O_2 and HF etching) processes. HF treatment cannot remove Ge–O bonds, so the Ge–O–Ge stretching signal at ~800 cm⁻¹ is still noticeable even after the two-step etching.

etching process, HF/ethanol aqueous solution was used to remove the amorphous GSO matrix, yielding freestanding SiGe NCs with surface hydride bonds (*i.e.*, $Si-H_x$ and $Ge-H_x$, Fig. 1d) which are available for further surface functionalization. Raman spectra of the composites show intense Ge–Ge, Si–Ge, and Si–Si optical phonons at 280, 399, and 483 cm^{-1}, respectively (Fig. 1e), qualitatively consistent with the preservation of the SiGe alloy after etching processes and in good agreement with the XRD results of the etched samples (Fig. 1c). However, all diffraction signals slightly shifted to a lower degree following the HF etching, indicating the lattice expansion of the crystals. The alloy composition was estimated to be $Si_{0.5}Ge_{0.5}$ based on Vegard's law (Table S1†), and the increase of Ge content is in good agreement with the partial removal of the surface Si atom during HF etching.[23]

For the typical functionalization reactions, ~150 mg of the freshly etched hydride-terminated SiGe NCs were added to the predesigned solution containing ligands and other precursors (*e.g.*, radical initiators), and the temperature was set to 65 °C to initiate the reactions. After the reaction, the solution containing ODE and etched SiGe NCs (ODE-capped SiGe NCs) changed from cloudy to semi-transparent. In contrast, the solution became almost transparent after the treatment with OAm (OAm-capped SiGe NCs). The functionalized SiGe NCs

were collected and purified by multiple washing steps (experimental details available in the ESI†).

No observable peak shift or broadening was observed from the XRD patterns of the ODE- or OAm-capped SiGe NCs, indicating that both functionalization approaches do not affect the average size of the Si/Ge compositional ratio of the particles (Fig. 2d and e). Although ODE can successfully passivate Si and Ge NCs *via* hydrosilylation and hydrogermanation,[24] in this study, the yield of the ODE-capped SiGe particles was noticeably low. Our observation suggested that ligands did not well passivate the SiGe surface through radical-initiated functionalization (Fig. 2c). This was further confirmed by the FT-IR results as more significant oxidation signals were found from the sample after ODE functionalization compared to the ML-capped SiGe NCs (Fig. 3a).

We reason that the significant difference in the effectiveness of the two general surface functionalization approaches may originate from the difference in the reaction rate. Compared to the fast reaction between the organoamine and the surface hydride,[18] radical-initiated hydrosilylation/hydrogermylation requires at least two rate-determining steps (RDSs), including the production of radicals from the decomposition of the initiator and the cleavage of hydride bonds and thus commonly takes a much longer time to com-
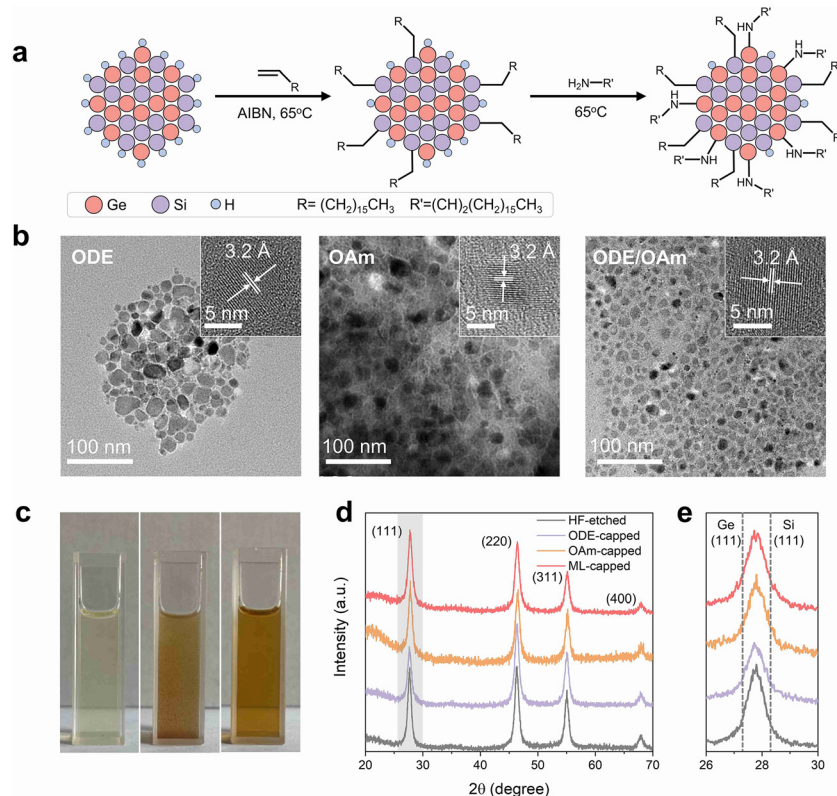

Fig. 2 Synthesis procedure and materials characterization of the functionalized NCs. (a) Schematic procedure of the two-step functionalization method of SiGe NCs (AIBN = 2,2′-azobis(2-methylpropionitrile)). (b) TEM and high-resolution TEM images of SiGe NCs after ODE, OAm, and two-step functionalization. (c) Photographs of the toluene solutions containing SiGe NCs capped by ODE, OAm, and ODE + OAm mixed ligands from left to right. (d) XRD patterns of SiGe NCs before and after ligand passivation. (e) XRD patterns corresponding to (d) in the range of 26°–30°. Dotted lines at 27.2° and 28.2° indicate the diffraction signals of the (111) facets of diamond-structured Ge and Si, respectively.
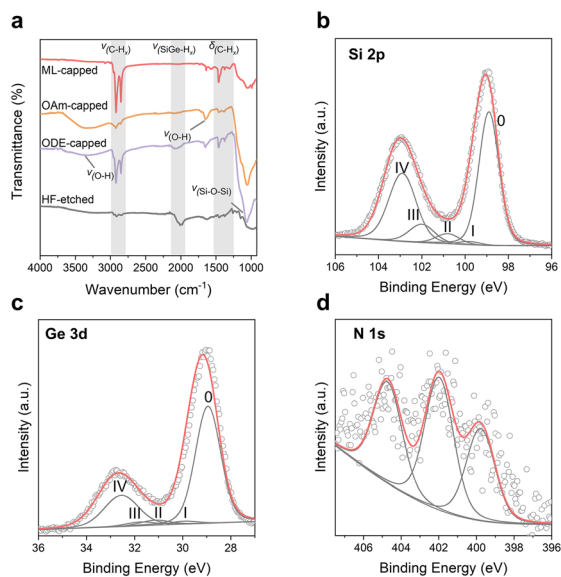
Fig. 3 Surface chemistry characterization of the functionalized NCs. (a) FT-IR spectra of the SiGe NCs before and after ligand passivation. (b–d) High-resolution X-ray photoelectron spectroscopy (XPS) results of ML-capped SiGe NCs. Silicon $2p_{1/2}$ and germanium $3d_{3/2}$ components are omitted for clarity.

Fig. 4 Photophysical properties of SiGe NCs functionalized using various ligands. (a) Absorption spectra and (b) PL emission spectra of SiGe NCs after ODE, OAm, and ML functionalization (excitation wavelength: 320 nm). (c and d) Time-resolved PL lifetime decays of emission peaks in the blue region (λ_{em} = 407–437 nm, excitation source: 365 nm pulse laser) and (d) in the NIR region. (λ_{em} = 763–779 nm, excitation source: 320 nm pulse laser.)

plete.[25] On the other hand, the surface hindrance increases following the anchoring of long aliphatic ligands and prohibits an effective interaction between the radical and the surface hydride—one of the RDSs of radical-initiated hydrosilylation/hydrogermylation. The unreacted surface hydride bonds Si–H_x and Ge–H_x were prone to oxidation when the purification was carried out in air, in agreement with the substantial Si–O and Ge–O signals from the ODE-capped sample.

Compared to ODE, OAm offers better surface coverage and solution dispersity of SiGe NCs as the interaction with organoamine and surface hydride does not require additional catalysts or radical initiators. However, after the OAm functionalization, an intense blue PL at 407 nm emerges from the OAm-capped sample with an average lifetime of 1.6 ns (Fig. 4b, c and Table S3†). Similar blue emission has also been found from the Si and Ge NCs after interacting with an amine or other nitrogen species and can be assigned to surface-species-induced radiative recombination.[18,26]

Motivated by the possibility in the mixed ligand passivation approaches on Si NCs and Ge NCs,[27,28] we sought to investigate an ML passivation approach to effectively passivate SiGe NCs by combining the benefits of both functionalization methods (*i.e.*, hydrosilylation/hydrogermylation and amine incorporation). We applied a radical imitated reaction with alkenes (*i.e.*, ODE in this study) for the first step of functionalization because alkyl-passivation does not generate any photo-active surface trap states on Si or Ge NCs.[24,25] As for the second step functionalization, OAm serves as the ligand to rapidly interact with the residual hydride bonds to further enhance surface ligand coverage. The concentration of the SiGe NCs after the ML functionalization approach is drastically
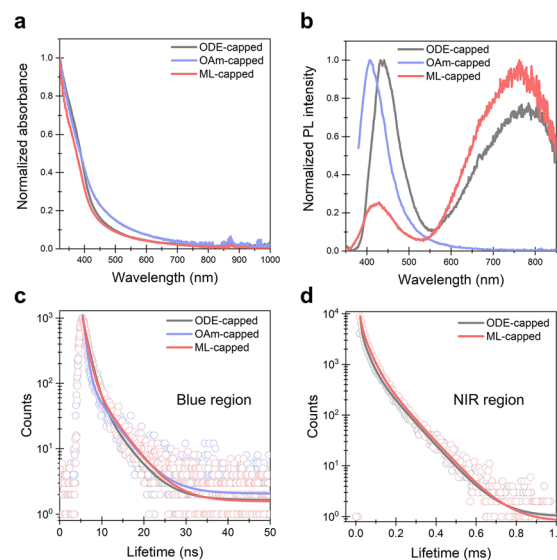
improved, and the surface oxide signal is substantially reduced in the FT-IR spectrum, suggesting the effective passivation of both ligands.

The morphology of the functionalized SiGe NCs is further revealed by transmission electron microscopy (TEM). Bright-field images confirm that all NCs passivated by various ligands are composed of highly crystalline cores with different shapes with average sizes over 10 nm (Fig. 2b and S2†). The elemental chemical environments were further investigated using high-resolution X-ray photoelectron spectroscopy (XPS) of ML-capped SiGe NCs. The characteristic signals centered at 98.9 eV of Si 2p and 29.0 eV of Ge 3d spectra can be assigned to the Si(0) and Ge(0) signals, indicating that the elemental alloy crystalline core of SiGe NCs is not affected by ML passivation.[24,28] The characteristic signals at 399.8 eV, 402.0 eV and 404.8 eV (Fig. 3b–d) are consistent with the anchored amine ligands and other germanium oxynitride species.[29,30]

To deepen the understanding of the potential influences of ligand passivation on the photophysical properties of SiGe NCs, we performed the absorption and photoluminescence (PL) measurements on the ODE-capped, the OAm-capped, and the ML-capped samples. All three samples show similar absorption features, which can be attributed to the SiGe crystalline core absorption (Fig. 4a). Prior to the ligand passivation, no PL was observed from H-SiGe NCs, possibly due to the abundant surface traps or potential particle passivation that quenches the PL, which was also found on Si and Ge NC systems.[19,24,31] When SiGe NCs are passivated by ODE, two new PL signals at 437 nm and 779 nm emerge with FWHM
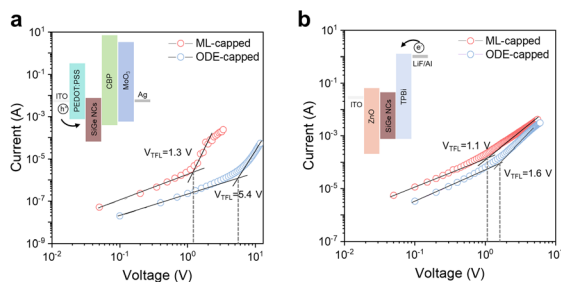
Fig. 5 Device architecture and SCLC results. Current–voltage curves for (a) hole-only and (b) electron-only devices under dark conditions. Inset figures show the device architecture for both types of devices. The fabrication details are available in the Experimental section in the ESI.† SCLC fitted results (solid lines) reveal the improved hole mobility and the trap-filling limit voltage (V_{TFL}), showing reduced trap densities of ML-capped SiGe NCs. Detailed numbers are available in Table S5.†

values of 73 nm and 236 nm, respectively (Fig. 4b). The blue-emitting and NIR PLs with average lifetimes of 1.92 ns and 59 μs can be contributed by the radiative recombination channels given by the surface Ge–O type defect states and the intrinsic bandgap, respectively (Fig. 4c, d and Table S4†).[16,32,33] The intense NIR emission of the SiGe NCs suggests that the ODE and OAm combination can effectively passivate the alloy surface without creating a substantial amount of nitrogen-based trap states.

To investigate the impact of the ML passivation on the electrical properties of SiGe NCs, we fabricated electron- and hole-only devices *via* solution-based processes (Fig. 5, see Experimental section in the ESI† for more details). The space-charge-limited current (SCLC) method was applied to estimate the carrier mobilities and trap densities of SiGe NCs (Fig. 5, calculation details available in the ESI†). The ML-capped SiGe NCs show 1.3 V and 1.1 V of trap-filled limit voltage (V_{TFL}) in hole-only and electron-only devices, substantially lower than the values of the ODE-capped SiGe samples (5.4 V and 1.6 V, respectively). The trap densities of ML-capped SiGe NCs were therefore calculated to be 5.2×10^{16} cm^{-3} (n_{te}) and 6.2×10^{16} cm^{-3} (n_{th}) through calculation (Table S5†), 1.3 and 3.7 times lower than in ODE-capped SiGe NCs (Fig. 5c). We also calculated the carrier mobilities based on the analyses of the current density–voltage (J–V) results using the Mott–Gurney equation (eqn (1) in the ESI†). According to the J–V curves, we obtained electron (μ_e) and hole (μ_h) mobilities of up to 6.3×10^{-6} cm^2 V^{-1} s^{-1} and 1.1×10^{-6} cm^2 V^{-1} s^{-1}, respectively, which are 1.2 and 2.2 times higher than the ODE-capped particles (Table S5†). We conclude that the ML passivation substantially reduces the surface trap states, yielding an improved charge carrier mobility performance in the SiGe NC thin films.

Conclusions

We report a mixed-ligand passivation approach that enables improved surface functionalization on SiGe alloy NCs.

Compared to conventional surface functionalization methods, this new approach allows alkene and amine ligands to interact effectively with surface Si–H and Ge–H bonds, yielding SiGe alloy particles with more dense surface ligand passivation and better solution stability. The efficient surface passivation on the alloy particle surfaces can further be evidenced by the enhanced intrinsic NIR emission, improved charge carrier mobilities, and reduced trap densities. This work demonstrated that the conventional surface functionalization approaches could be extended to passivated complicated alloy surfaces and provides an approach that can be used to prepare stable and concentrated "inks" for solution-processable SiGe-alloy-based optoelectronics.

Conflicts of interest

The authors declare no conflict of interest.

Acknowledgements

References

1 S. Regli, J. A. Kelly, A. M. Shukaliak and J. G. Veinot, *J. Phys. Chem. Lett.*, 2012, **3**(13), 1793–1797.

2 R. J. Clark, M. Aghajamali, C. M. Gonzalez, L. Hadidi, M. A. Islam, M. Javadi, M. H. Mobarok, T. K. Purkait, C. J. T. Robidillo, R. Sinelnikov, A. N. Thiessen, J. Washington, H. Yu and J. G. C. Veinot, *Chem. Mater.*, 2016, **29**(1), 80–89.

3 Q. Li, T.-Y. Luo, M. Zhou, H. Abroshan, J. Huang, H. J. Kim, N. L. Rosi, Z. Shao and R. Jin, *ACS Nano*, 2016, **10**(9), 8385–8393.

4 H. Chen, J. Xu, Y. Wang, D. Wang, R. Ferrer-Espada, Y. Wang, J. Zhou, A. Pedrazo-Tardajos, M. Yang, J.-H. Tan, X. Yang, L. Zhang, I. Sychugov, S. Chen, S. Bals, J. Paulsson and Z. Yang, *ACS Nano*, 2022, **16**(9), 15450–15459.

5 D.-J. Xue, J.-J. Wang, Y.-Q. Wang, S. Xin, Y.-G. Guo and L.-J. Wan, *Adv. Mater.*, 2011, **23**(32), 3704–3707.

6 S. Assefa, F. Xia and Y. A. Vlasov, *Nature*, 2010, **464**(7285), 80–84.

7 R. Pillarisetty, *Nature*, 2011, **479**(7373), 324–328.

8 L. M. Wheeler, A. W. Nichols, B. D. Chernomordik, N. C. Anderson, M. C. Beard and N. R. Neale, *Nano Lett.*, 2016, **16**(3), 1949–1954.

9 G. Palfinger, B. Bitnar, H. Sigg, E. Müller, S. Stutz and D. Grützmacher, *Phys. E*, 2003, **16**(3–4), 481–488.

10 Y. S. Tang, S. Cai, G. Jin, J. Duan, K. L. Wang, H. M. Soyez and B. S. Dunn, *Appl. Phys. Lett.*, 1997, **71**(17), 2448–2450.

11 C.-W. Hwang, M.-K. Ryu, K.-B. Kim, S.-C. Lee and C.-S. Kim, *J. Appl. Phys.*, 1995, **77**(7), 3042–3047.

12 S. Takeoka, K. Toshikiyo, M. Fujii, S. Hayashi and K. Yamamoto, *Phys. Rev. B: Condens. Matter Mater. Phys.*, 2000, **61**(23), 15988–15992.

13 Y. M. Yang, X. L. Wu, G. G. Siu, G. S. Huang, J. C. Shen and D. S. Hu, *J. Appl. Phys.*, 2004, **96**(9), 5239–5242.

14 X. D. Pi and U. Kortshagen, *Nanotechnology*, 2009, **20**(29), 295602.

15 E. J. Henderson and J. G. C. Veinot, *Chem. Mater.*, 2007, **19**(8), 1886–1888.

16 S. D. Barry, Z. Yang, J. A. Kelly, E. J. Henderson and J. G. C. Veinot, *Chem. Mater.*, 2011, **23**(22), 5096–5103.

17 M. Y. Bashouti, K. Sardashti, S. W. Schmitt, M. Pietsch, J. Ristein, H. Haick and S. H. Christiansen, *Prog. Surf. Sci.*, 2013, **88**(1), 39–60.

18 M. Dasog, Z. Yang, S. Regli, T. M. Atkins, A. Faramus, M. P. Singh, E. Muthuswamy, S. M. Kauzlarich, R. D. Tilley and J. G. C. Veinot, *ACS Nano*, 2013, 7(3), 2676–2685.

19 M. Javadi, V. K. Michaelis and J. G. C. Veinot, *J. Phys. Chem. C*, 2018, **122**(30), 17518–17525.

20 J. M. Buriak, *Chem. Rev.*, 2002, **102**(5), 1271–1308.

21 E. J. Henderson, M. Seino, D. P. Puzzo and G. A. Ozin, *ACS Nano*, 2010, **4**(12), 7683–7691.

22 E. J. Henderson, C. M. Hessel, R. G. Cavell and J. G. C. Veinot, *Chem. Mater.*, 2010, **22**(8), 2653–2661.

23 J. G. Veinot, *Chem. Commun.*, 2006, **40**, 4160–4168.

24 M. Javadi, D. Picard, R. Sinelnikov, M. A. Narreto, F. A. Hegmann and J. G. C. Veinot, *Langmuir*, 2017, **33**(35), 8757–8765.

25 Z. Yang, C. M. Gonzalez, T. K. Purkait, M. Iqbal, A. Meldrum and J. G. Veinot, *Langmuir*, 2015, **31**(38), 10540–10548.

26 H. Chen, J. Xu, Y. Wang, D. Wang, R. Ferrer-Espada, Y. Wang, J. Zhou, A. Pedrazo-Tardajos, M. Yang, J. H. Tan, X. Yang, L. Zhang, I. Sychugov, S. Chen, S. Bals, J. Paulsson and Z. Yang, *ACS Nano*, 2022, **16**(9), 15450–15459.

27 M. Locritani, Y. Yu, G. Bergamini, M. Baroncini, J. K. Molloy, B. A. Korgel and P. Ceroni, *J. Phys. Chem. Lett.*, 2014, **5**(19), 3325–3329.

28 M. A. Islam, R. Sinelnikov, M. A. Howlader, A. Faramus and J. G. C. Veinot, *Chem. Mater.*, 2018, **30**(24), 8925–8931.

29 M. Dasog, G. B. De Los Reyes, L. V. Titova, F. A. Hegmann and J. G. C. Veinot, *ACS Nano*, 2014, **8**(9), 9636–9648.

30 J. J. Romero, M. L. Dell'arciprete, H. B. Rodríguez, E. Gonik, D. Cacciari, A. L. Moore and M. C. Gonzalez, *ACS Appl. Nano Mater.*, 2022, **5**(6), 8105–8119.

31 M. Lai, Y. Zhang, L. Zhao, Y. H. Huang, L. Zhang, W. Fu, P. Chen, X. D. Wang, T. Zhu and Z. Yang, *Angew. Chem., Int. Ed.*, 2023, **62**(26), e202304056.

32 P. K. Giri and S. Dhara, *J. Nanomater.*, 2012, **2012**, 1–5.

33 M. Zacharias and P. M. Fauchet, *Appl. Phys. Lett.*, 1997, **71**(3), 380–382.